**Proceedings of the ASME 2019 38th International Conference on Ocean, Offshore and Arctic Engineering**
**OMAE2019**
**June 9-14, 2019, Glasgow, Scotland, UK**

# OMAE2019-96034

# ON MOTION AND HYDROELASTIC ANALYSIS OF A FLOATING OFFSHORE WIND TURBINE

**Azin Lamei**
Civil Engineering Department
University of Dundee
Dundee, DD1 4HN, UK

**Masoud Hayatdavoodi**
Civil Engineering Department
University of Dundee
Dundee, DD1 4HN, UK
Email: mhayatdavoodi@dundee.ac.uk

**Carlos Wong**
CBJ-Kaluosi-Qianghai Group
338 Hennessy Road, Wanchai
Hong Kong

**Bin Tang**
College of Shipbuilding Engineering,
Harbin Engineering University,
Harbin, China

## ABSTRACT

*This study is concerned with motion analysis and hydroelastic response of a floating offshore wind turbine to wave loads. The novel floating structure, made of prestressed concrete, is designed to support multiple wind turbines, and it rotates according to the environmental loads to face the incoming wind. The floating structure is attached to a mooring line that allows the rotation of the structure in response to the environmental loads. The floating structure is an equilateral triangular platform. The wind turbines are located at the vertices. Due to the dimensional characteristics of the structure, elasticity of the floating platform plays an important role in its dynamics. While the dynamic response of the structure is driven by both aerodynamic and hydrodynamic loads, this study focuses on the motion and elastic response of the novel floating structure to the hydrodynamic loads only. The three dimensional hydrodynamic loads on the floating structure are obtained by use of the constant panel approach of the Green function method, subject to linear mooring loads. A finite element analysis is carried out for the calculation of the elastic response of the structure. Computations of the integrated linear structure-fluid-structure interaction problem are performed in frequency domain using HYDRAN, a computer program written for the linear dynamic analysis of rigid and flexible bodies. Results presented here include the response amplitude operators of both the rigid and flexible bodies to incoming waves of various frequencies and directions. Also presented are the wave-induced stresses on the floating body, and the elastic deformations.*

## Introduction

Environmental pollutants and the increasing need of energy, has led the policy-makers to seek for substi-

tutes of fossil-fuel energy supplies. As reported by [1], wind energy by the end of year 2015, has reached to 7% of the total global power generation with the capacity of 435 GW, where the share of onshore and offshore sites are 420 GW and 12 GW, respectively. Wind energy harvested mainly onshore, has been globally recognised as one of the best solutions among other renewable energies to meet the energy needs. However, due to the limited availability of onshore lands, visual and noise disturbances, offshore wind energy is gaining more interest. Offshore wind energy, with more consistent and stronger wind speeds is shown to be a promising wind resource for energy production. Among various options for the offshore wind, floating wind turbines offer some advantages, namely the ability to install offshore wind turbines at deep waters, independent of the seabed and far from the coastal populated areas. Offshore wind turbines whether fixed or floating can benefit from the mature technology of onshore wind turbines and the oil and gas development at offshore platforms.

To develop a floating offshore wind turbine (FOWT), certain challenges regarding the platform and its installation need to be met, such as proper mooring lines and anchors suitable for the seabed, grid connection and the operation and maintenance activities. The dynamics of a FOWT is based on simultaneous effect of both wind and water loadings. Hence, it is essential to consider the aero- and hydrodynamic loads simultaneously. The motion of the floater is of great importance as it determines the wind turbine direction to the wind and the pressure distribution on the rotor blades. As a result, all these challenges increase the cost of electricity production by a FOWT. Several extensive reviews about FOWTs, and the developed numerical coupling tools can be found for example in [2, 3].

The platforms developed for a FOWT, can be classified into two categories, namely single wind turbine floater or multi-wind-turbine floaters. Several concepts for the single wind turbine substructure are suggested, for instance spar buoys, semi-submersibles and TLP, generally based on the approach that the stability of the floater is achieved, see e.g. [4, 5]. Multi-wind-turbine floaters based on semi-submersible platform concept, can result in cheaper configuration for FOWTs with common mooring lines and less motion of the floater. However, the spacing of the turbines on the floater is a challenge to minimize the interaction of the rotor wakes. Until recently, several multi-wind-turbine concepts have been suggested, addressing the challenges of tracing the dominant wind turbine and the mooring lines of the whole floater, see e.g. [6] and [7].

Analysis of the motion of multi-floater platforms, however, is more challenging due to the relative size of the structure and the effect of multiple wind turbines. To predict accurately the motion of the whole structure, a numerical tool is needed to account for all the coupling effects of the loads acting on the system. In this paper, the goal is to perform a preliminary study of a novel semi-submersible triangular floater suggested by [7], where three similar wind turbines are installed at each vertice of the triangle. In the presented simulations, as an initial step we start with hydrodynamic loads on the floater. Here only the moored platform is considered and the wind turbines, the effect of the induced motion by the currents and the wind load will be discussed in the future. This study is concerned with the hydroelastic response of the platform when subjected to regular waves. Larger dimensions of multi-floater platforms may introduce a subset of low natural frequencies that may effect the loads experienced by the floater. Therefore, dynamic effects influenced by the platform elasticity will come to play. The wave-structure interaction and elastic response of the substructure is implemented within linear diffraction theory. The inclusion of the elasticity of the substructure is based on an explicit formulation of stiffness matrix considering both internal stresses and external hydrostatic pressure. Thus, with this analysis, the equation of motion including the substructure flexible modes will be derived. Finally dynamic responses considering the regular wave and the structural deformation of the platform are computed.

First, the novelty and the configuration of the floater is illustrated. Then the applied theory to obtain the elastic responses of the floater together with the results and conclusion are given. In this study, only the moored platform with no wind turbines is considered i.e. in the current analysis the mass matrix is only based on the platform and the ballast weight. The interaction of the substructure and the fluid is determined with the application of linear wave theory solved in frequency domain. Further, structural responses of the platform are determined using finite element method, and the

stresses and displacements are reported in frequency domain.

### The platform configuration

A semi-submersible platform concept is introduced by [7] assuming both triangular and trapezoidal shapes, supporting three or five wind turbines, respectively. The substructure suggested to be of pre-stressed concrete, consists of floaters supporting the wind turbines and several pontoons connecting the floaters together. Within this configuration, the construction cost will be substantially less than single turbine floaters. The distance between turbines i.e. the length of the pontoons, is mainly driven by the wake effect of the turbines. The optimum distance between the rotor center of the turbines with a rotor diameter $D$, is approximated to be $2.2D$ where the two rows of the turbines are located in staggered manner to minimize the rotor wake interaction, [7].

The novelty of this platform lies in the turning mechanism to trace the dominant wind. The cable lines connected to each of the floaters are merged to a single point in deeper depth. The merging point is connected to an anchor at the seabed with a mooring line. The floater rotates in response to the environmental loads to face the rotors to the strongest wind direction. The mooring line attached to the anchor is pre-tensioned to submerge the floater to the desired draft as well as being able to withstand the wind loads on the turbine, wave loads on the floater and the current effects.

In this study, the focus is on an equilateral triangular platform, where the two turbines are placed in a row at the windward and one turbine at the leeward. A rendered view of the structure and the characteristic dimensions of the platform are shown in Fig. 1. The rotor diameter is assumed to be 120 m with the pontoons each with the length of 250 m. The pontoons are assumed to be concrete beams with hollow circular sections submerged at 16 m below the still water level (SWL). The diameter of the floater and the pontoons are 14 m and 8 m, respectively. The thickness of the columns is 0.4 m and for the pontoons it is 0.35 m.

### The hydroelastic theory

The applied theory to determine elastic responses of the floating substructure is based on linear wave

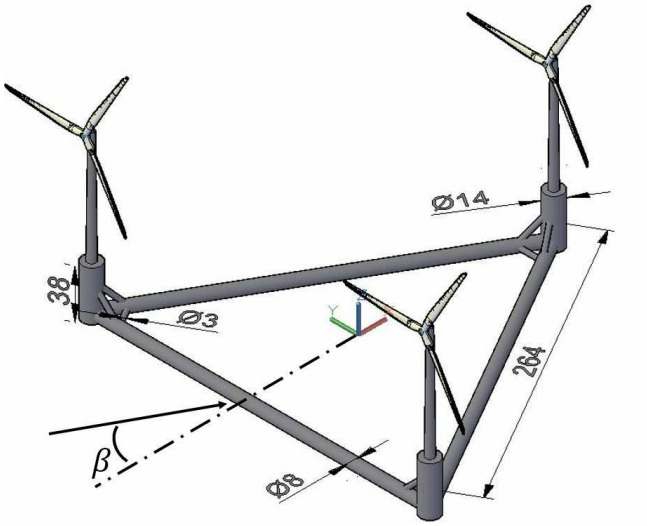


**FIGURE 1**. The triangular semi-submersible platform. All dimensions are in meters.

diffraction and three dimensional linear hydroelasticity. Hydrodynamic loads on the body are obtained using linear wave diffraction theory, wherein the fluid is assumed to be incompressible and inviscid, and the flow is irrotational. The linear diffraction theory together with the derivation of its relations are thoroughly explained in [8] and [9], for example. In linear wave diffraction theory, the body and free surface boundary conditions are satisfied to the first order. The velocity field is represented by the gradient of the velocity potential, satisfying Laplace's equation, $\nabla^2\phi = 0$, where $\phi$ is the frequency domain velocity potential of the flow around the structure.

For all the degrees of freedom of the structure, the total velocity potential is expressed as:

$$\phi = \phi_R + \phi_D, \quad \phi_D = \phi_I + \phi_{scattering}, \tag{1}$$

where $\phi_D$ is the solution for the fixed body, regarding the incident ($\phi_I$) and the scattered waves. The scattering component ($\phi_{scattering}$) represents the disturbance of the incident waves by the fixed body. Moreover, $\phi_R$ is the radiation potential due to the body motion and $\phi_j$ is the unit–amplitude radiation potential. Since the problem is linear, the total velocity potential can be represented by a superposition of different modes:

$$\phi_R = \sum_{j=1}^{6+M_p} \xi_j \phi_j, \tag{2}$$

where $M_p$ is the total number of the structure degrees of freedom and 6 represents the rigid body degrees of freedom. $\xi_j = |\xi_j| e^{\mathrm{i}\omega t}$ is the complex body displacement phasor. The radiation and diffraction velocity potentials are determined considering the following boundary conditions on the body surface.

$$\begin{cases} \dfrac{\partial \phi_j}{\partial n} = \mathrm{i}\omega n_j, \quad \text{for } j = 1, 2, \cdots 6 + M_p. \\ \dfrac{\partial \phi_D}{\partial n} = 0 \end{cases} \tag{3}$$

To obtain the velocity potentials, one approach is by the application of source distribution over the mean wetted body surface, where the source strength is equal to the normal velocity on the surface, [10]. Boundary value problems as mentioned shortly earlier, can be solved by describing the source potentials with Green's function. Typically the integral equations for radiation and diffraction problems with Green's function are evaluated with panel methods otherwise referred to as boundary element methods (BEM). In BEM, the geometry is descretized in either flat or curved panels to find the source strength via the integrals.

The forces and moments on the body are represented as a superposition of the forces when the body is fixed and exposed to the incident waves and when the body is oscillating in an otherwise calm water. The forces and moments on the body when the structure is fixed in its place exposed to incident waves, are called *wave excitation*, ($F_{excitation}$) loads, see e.g. [9].

The total load on a floating structure is given by the sum of the external hydrodynamic pressure forces, hydrostatic restoration forces and mooring line loads, and wave excitation forces. The pressure forces include radiation forces and excitation forces. Thus, Newton's second law takes the form:

$$\begin{aligned} (F_j)_{\text{tot}} &= (F_j)_{\text{restoring}} + (F_j)_{\text{hydro}} + (F_j)_{\text{excitation}} \\ &= -\omega^2 M_{jk} \xi_k, \quad j,k = 1, 2, \cdots 6 + M_p, \end{aligned} \tag{4}$$

where $M_p$ is the total number of degrees of freedom of the structure and standard indicial notation is used implying summation over repeated indices. Here $\omega$ is the angular wave frequency, $M_{jk}$ is the linearized body inertia matrix and $\xi_k$ is the complex body response phasor in mode k, however in the frequency-domain analysis, the amplitude of the response ($|\xi_k|$) is applied.

Restoring forces, $F_{\text{restoring}}$, represent the hydrostatic and mooring loads on the body. $F_{\text{hydro}}$ and $F_{\text{excitation}}$ are the hydrodynamic and wave excitation forces on the body.

The pressure forces on the structure are computed with the linearized Bernoulli equation:

$$F_i = \iint_{S_b} \rho\, n_i dS = -\rho \iint_{S_b} (\mathrm{i}\omega\phi + g z) n_i \, dS, \tag{5}$$

where $F_i$ is the pressure force, $\rho$ the fluid density, $n_i$ the normal vector on the panel on the body, $S_b$ the body wetted surface, $\omega$ the wave frequency and $g$ is the gravity. By substituting radiation or incident and diffraction velocity potentials respectively, hydrodynamic and wave excitation loads are determined. Hydrodynamic loads are expressed as a decomposition of the sinusoidal force into components in phase with the velocity and acceleration of the corresponding mode. Due to the forced motion of the structure in the absence of incident waves, outgoing waves from the body are generated. The forced motion results in oscillating fluid pressure on the body surface. Integrating the fluid pressure on the body surface gives hydrodynamic added mass and damping loads. Further, to compute the wave excitation loads, Haskind relations are applied, [8].
Consistent with linear theory in the frequency domain, the equation of motion can be written as follows:

$$\left(-\omega^2 M_{jk} - \omega^2 a_{jk} + \mathrm{i}\omega b_{jk} + c_{jk}\right) \xi_k = A X_j, \tag{6}$$

where $a_{jk}$ is the added mass, $b_{jk}$ the wave damping coefficient and $X_j$ is the amplitude of wave excitation

force in complex notation, normalized per wave amplitude in mode $j$. Moreover, $A$ is the wave amplitude and $c_{jk}$ is the restoring force coefficient, influenced by both hydrostatic and mooring forces.

For a flexible body, the natural frequencies will fall within the wave spectrum and results in deformational degrees of freedom. Thus, linear hydroelasticity analysis following the linear potential theory, is based on extending the degrees of freedom with generalized modes to include the deformation of the body. In this case, the hydrostatic coefficient will be modified to account for the internal loads of the structure as well as the external loads on the body. To compute the hydrostatic stiffness, the complete formulation developed by [11] is applied in which the effect of fluid pressure as well as structural geometric stiffness are considered.

The stiffness matrix computed by initial stresses is referred to as geometric or initial stress stiffness matrix:

$$c_f = c^f + c^g, \tag{7}$$

where $c_f$ is the hydrostatic stiffness. $c^f$ and $c^g$ are the components resulting from external and internal forces, respectively. The complete hydrostatic stiffness is computed as follows:

$$\begin{aligned} c_{f,ij} &= -\rho g \int_{S_b} \phi_k^i (\phi_3^j + z\,\varepsilon_v^j)\, n_k\, dS \\ &+ \rho g \int_{S_b} z \phi_l^i\, \phi_{k,l}^j\, n_k\, dS + \int_{\Omega_s} \sigma_{lm} \phi_{k,l}^i \phi_{k,m}^j\, n_k d\Omega, \\ & q,l,m = 1,2,3, \quad i,j = 1,2,\cdots N, \end{aligned} \tag{8}$$

in which $\rho$ is the mass density of the water, $g$ is the gravitational acceleration, $S_b$ is the wetted surface. $\phi_k^i$ is the velocity potential for mode $i$, representing the rigid body degrees of freedom for $i = 1,2,\cdots,6$ and deformational modes for $i > 6$. $n_k$ is the $k$-th component of the normal vector on the wet surface. The $\Omega_s$ is the structural volume, $\sigma_{lm}$ is the structural stress under gravitational loads in calm seas, $\varepsilon_v^j$ is the strain in mode $j$ and $z$ is the third component of the node coordinates pointing upwards. The first two integrals present the hydrostatic restoring coefficient and the last one is the geometric stiffness coefficient. Thus, the equation of motion, Eq. (6) in the frequency domain for wave frequency $\omega_q$ changes into:

$$\begin{aligned} &\xi_j[-\omega_q^2(M_{ij} + a_{f,ij}) + i\omega_q(b_{f,ij} + B_{s,ij}) + (C_{s,ij} + c_{f,ij})] \\ &= AX_i, \end{aligned} \tag{9}$$

where $M_{ij}$, $B_{s,ij}$ and $C_{s,ij}$ are the structural mass, damping and stiffness matrices, respectively and $a_{f,ij}$, $b_{f,ij}$ and $c_{f,ij}$ are the added mass, hydrodynamic damping and hydrostatic stiffness coefficients. $X_i$ is presented in complex notation, the amplitude of wave excitation force with wave amplitude $A$, and $\xi_j$ is the complex body response phasor in mode $j$. Note that to obtain the structural properties, i.e. natural dry frequencies, modal displacement and structural stiffness, first a finite element analysis is performed.

Considering the structural responses of a flexible body, for each degree of freedom that causes the displacement of the wet surfaces, the radiation potential problem should be solved. For large number of structural degrees of freedom, the computation is significantly time consuming. To tackle this problem, the structural deflection is presented by a superposition of simpler mathematical orthogonal mode shapes which are sufficiently general to represent the physical motion. For instance, the deflection of a floating body can be expressed by the free undamped wet bending modes of the body in the water or by the dry modes of the same structure in air, see for example [12]. Thus, the displacement of the body can be presented by a linear combination of these mode shapes with no loss in accuracy. For slow varying loads, the structural response is dominated by lower natural frequencies. A modal superposition of a reduced basis of the degrees of freedom will be chosen to solve the equation of motion.

#### Numerical set-up

The load distribution and the structural responses of the platform is obtained using a potential flow solver, namely HYDRAN [13]. HYDRAN, determines the hydroelastic responses of offshore floating bodies by integrating the structural finite element analysis with hydrodynamic computations, [14, 15]. For this problem, first, the platform is modelled with linear, elastic shell finite elements. With the reduced order vector based

on dry natural frequencies, dry modes of the structure is formulated and the eigen-frequencies and eigenvectors are obtained. Within this step, the stresses at the user defined points and mode shapes of the body are computed. The structural stiffness accounting for both internal forces of the platform and the hydrostatic stiffness effects of the fluid is determined. Then, the equation of motion in linear wave diffraction theory, with the computed stiffness matrix are solved. To numerically solve the equation of motions, the finite element model of the structure is mapped into panel mesh such that the structural mesh is conformed one by one to the hydrodynamic mesh. For hydrodynamic analysis, linear diffraction wave theory is applied and constant panel method where Green's function is used to solve the equation of motion.

The water depth is 200 m and as suggested by the design specifications of the platform, the draft is assumed to be 16 m. With the specified draft, the ballast is computed to be 75.54% of the internal volume of the pontoon to be filled in with water. The ballast is divided by the number of the pontoons and is assumed to be in closed compartments located at the middle of the pontoons. The length of each compartment is computed, $l_{ballast} = 199.70$ m. The weight of the ballast in each pontoon is distributed in all the points within the compartments. The tensioned mooring lines are modelled with cable joint elements in HYDRAN. The merging point of the mooring lines is at the center of the geometry and 50 m below the structure.

The simulations are performed for four wave heading angles, $\beta = 0^\circ$, $30^\circ$, $45^\circ$ and $90^\circ$ and wave frequencies varying between 0.084 to 0.2 Hz. The wave frequencies are chosen for a site at North Sea, see [16] for more details. Wave heading angle is defined as the angle between the incident wave in anti-clockwise direction with respect to the *x* axis. First, a mesh convergence study is performed to evaluate the optimum mesh size for the simulation.

### Mesh convergence study

To find the optimum element size for hydrodynamic analysis of the platform, three different grid sizes as fine mesh, 0.014 m/m $\times$ 0.014 m/m, medium mesh 0.018 m/m $\times$ 0.018 m/m and coarse mesh 0.020 m/m $\times$ 0.020 m/m are considered. The grid sizes are normalized by the length of the pontoons, that is 250 m. The wave induced responses for the rigid platform in headseas are obtained and compared together.

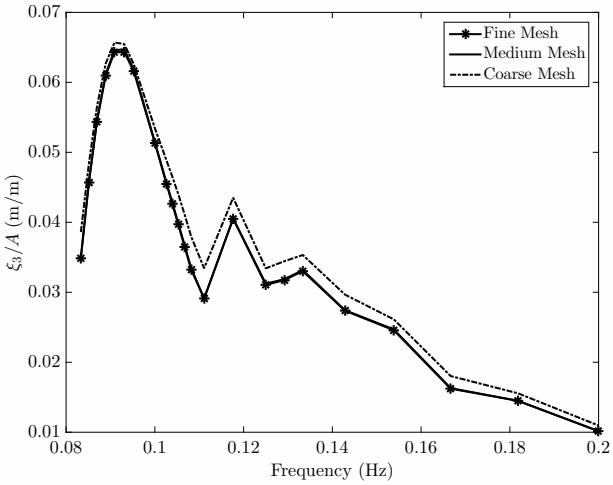


**FIGURE 2**. Comparison of the heave response of the floater with three different gird sizes in headseas, ($\beta = 0^\circ$).

Figure 2 shows the heave responses of rigid structure in head seas, with the aforementioned three grid sizes. The computed heave response of the medium mesh agrees well with the response obtained by using a fine mesh. However, considering the coarse mesh, higher response amplitude operators (RAOs) for wave frequencies larger than approximately 0.1 Hz are observed compared to heave RAO obtained with fine and medium mesh. Therefore, the converged grid size for these computations is 0.018 m/m $\times$ 0.018 m/m, with 11447 quadrilateral thin shell elements, and 11468 nodes. Using this mesh configuration, the computations take about three and half hours on a desktop computer with Intel Core i5 6500U, 3.20Ghz CPU and 32 GB memory.

### Results & Discussion

In the following sections, the structural responses of the platform as rigid and flexible bodies are computed and compared with each other. Within this comparison, the importance of considering elasticity for this platform will be presented. Vertical displacements and the stresses at some critical points on the platform are reported as well. Both rigid and flexible platforms are considered in this study. Results include response amplitude operators (RAO), vertical displacements and

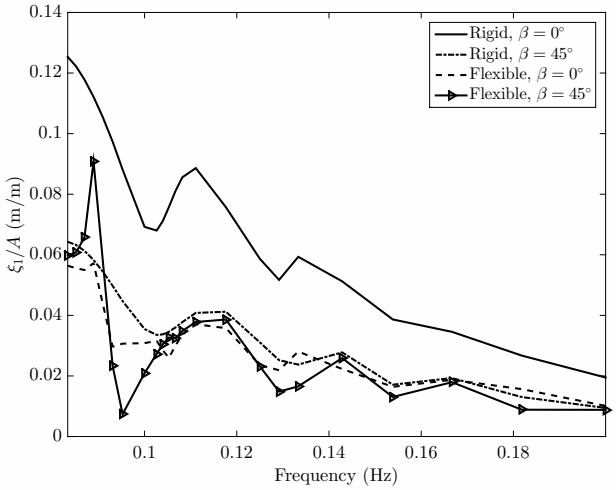


**FIGURE 3**. Comparison of RAOs for flexible and rigid bodies in surge for two incoming wave angles

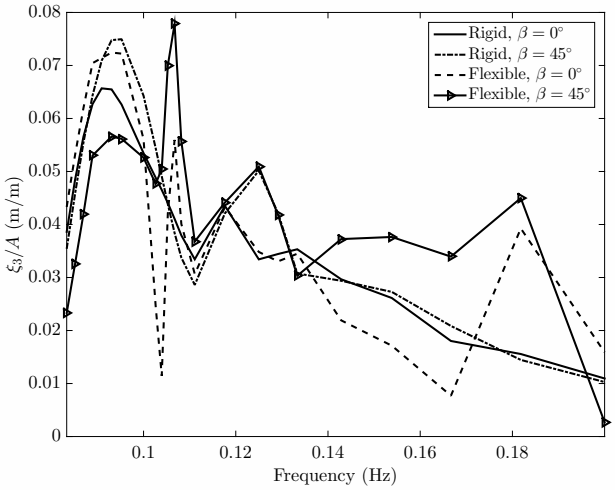


**FIGURE 4**. Comparison of RAOs for flexible and rigid bodies in heave for two incoming wave angles.

stresses versus wave frequency. Figures 3, 4, 5 and 6 present the predicted RAOs for two wave heading angles over the wave frequency for the sure ($\xi_1$) , heave ($\xi_3$), pitch ($\xi_5$) and yaw ($\xi_6$), respectively.

In Fig. 3, the RAOs in head seas for the rigid body are the largest values. However, for the second wave heading angle, $\beta = 45°$, both RAOs predicted for rigid and flexible bodies are similar. Figure 4 presents the comparison of RAOs in heave degree of freedom. For both wave heading angles, the responses are in the same order, while for $\beta = 45°$, the responses have more oscillations compared to the head seas. It can be seen that for heave degree of freedom, considering the elasticity, did not make significant changes into the response. However, the obtained responses in surge are different in magnitude for rigid and flexible platforms.

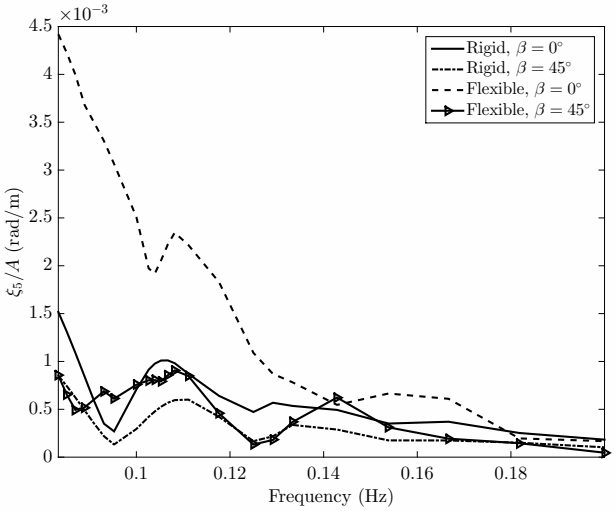


**FIGURE 5**. Comparison of RAOs for flexible and rigid bodies in pitch for two incoming wave angles.

Comparing the RAOs in pitch, Fig. 5 and yaw Fig. 6, the structure experiences larger motions in pitch degree of freedom. The computed RAO for the flexible platform with waves in $\beta = 45°$ are significantly higher than other presented responses. The calculations suggest almost zero responses in yaw for the rigid body whereas the RAO for flexible platform reach up to $4.5 \times 10^{-4}$ (rad/m) in $\beta = 45°$.

To obtain the vertical displacement at the three columns, the points in the perimeter of the floaters cross-sections furthest away from the center of the platform are considered. The columns are numbered as illustrated in Fig.7.

The vertical displacements for two wave heading angles in both rigid and flexible bodies are presented in Figs. 8, 9 and 10. Pitch and heave responses of the platform and the modal displacement at these points determined in the structural analysis, influence the final vertical displacement of the specified points. In all cases the computed responses for the rigid body motion is less than that of the flexible body, since the structural responses of the body are neglected. Moreover, comparing the response at the three points, the highest displacement in magnitude is observed at column

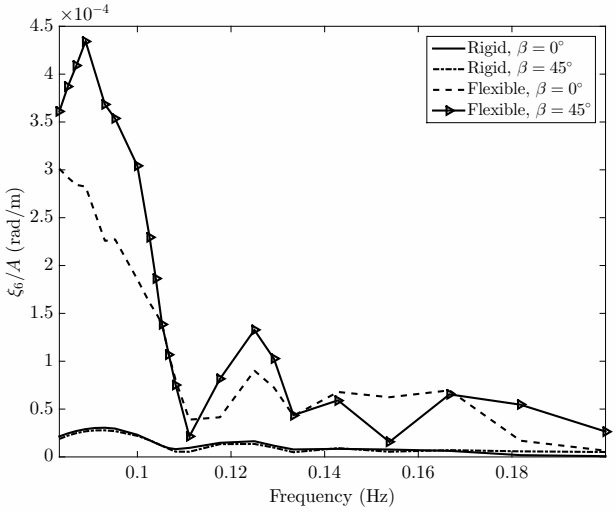


**FIGURE 6**. Comparison of RAOs for flexible and rigid bodies in yaw for two incoming wave angles.

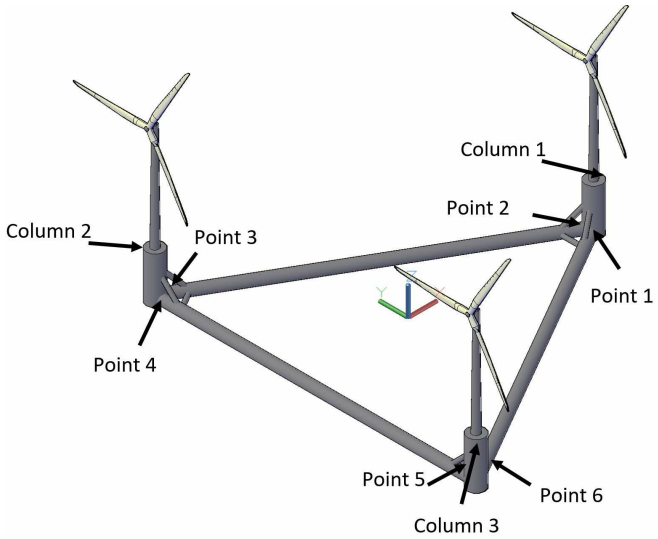


**FIGURE 7**. Isometric view of the structure, showing points that are chosen for vertical displacement and shear stress calculations.

1, outside of the rear wind turbine with wave heading angle 90°.

The shear stresses ($\sigma$) are also evaluated at the specified points on the platform demonstrated in Fig. 7. For this study, the points joining the pontoons to the floater are assumed to withstand considerable structural stresses. Thus, the stresses at these points are determined considering the platform as a flexible structure. The computed shear stress at the joining points around

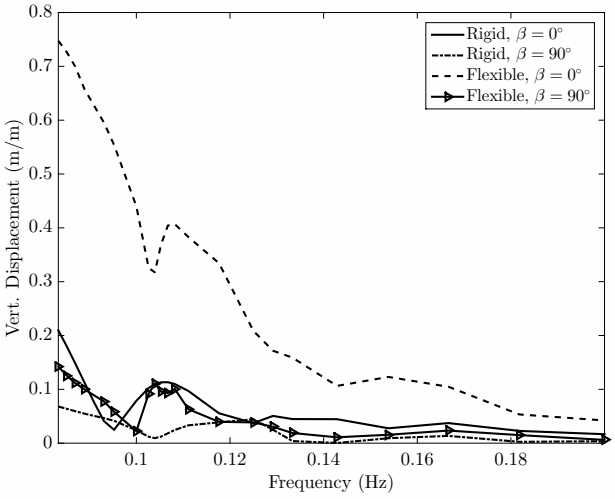


**FIGURE 8**. Vertical displacement of column 1 (shown in Fig. 7) for two incoming wave angles.

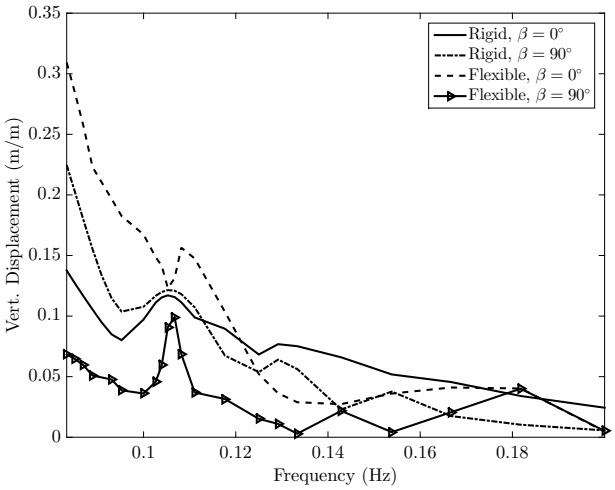


**FIGURE 9**. Vertical displacement of column 2 (shown in Fig. 7) for two incoming wave angles.

the front columns, Columns 2 and 3, are shown in Figs. 12 and 13, respectively. The shear stresses are smaller at points 3, 4, 5 and 6 compared to points 1 and 2 at the Column 1, Fig. 11. For wave heading angle $\beta = 90°$, both points 2 and 6 experience the peak in structural stresses. However, on column 2, the stresses for both points are approximately close in magnitude. Comparing the peaks predicted for the six points, point 2 experiences the largest shear stress. Depending on the properites of the concrete matrix, the yield strength is different, see e.g. [17] for more information. We note that the column thickness is 0.4 m in these calculations.

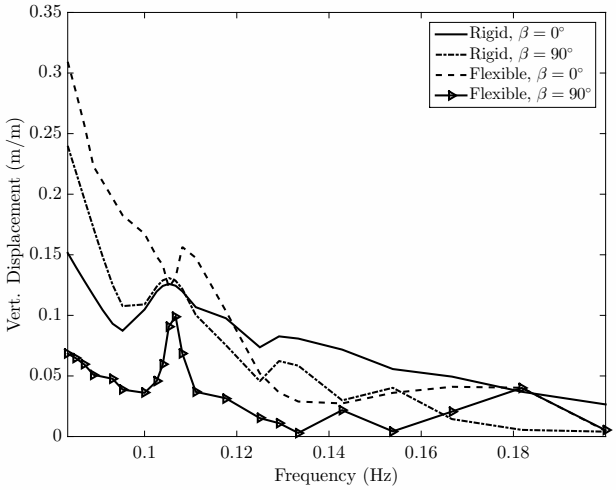


**FIGURE 10**. Vertical displacement of column 3 (shown in Fig. 7) for two incoming wave angles

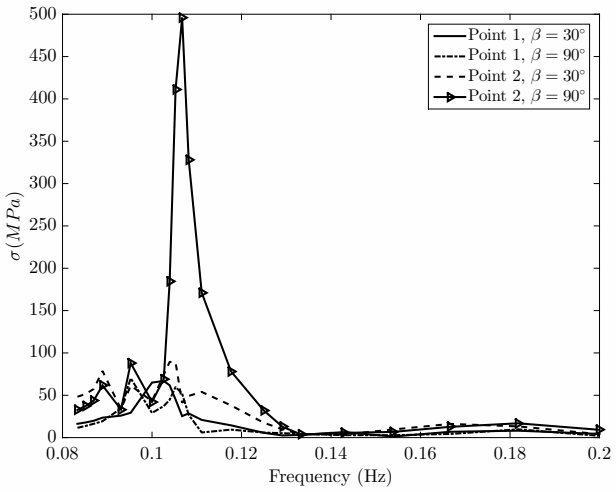


**FIGURE 11**. Structural stress computed at point 1 & 2 (Shown in Fig.7) for two incoming wave angles, illustrated in Fig.7.

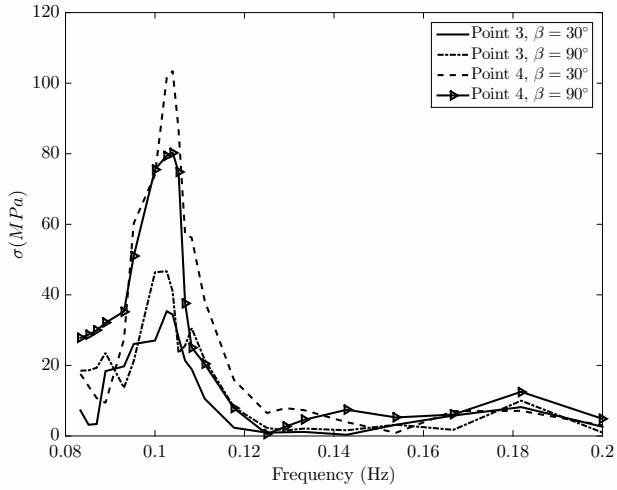


**FIGURE 12**. Structural stress computed at point 3 & 4 (Shown in Fig.7) for two incoming wave angles.

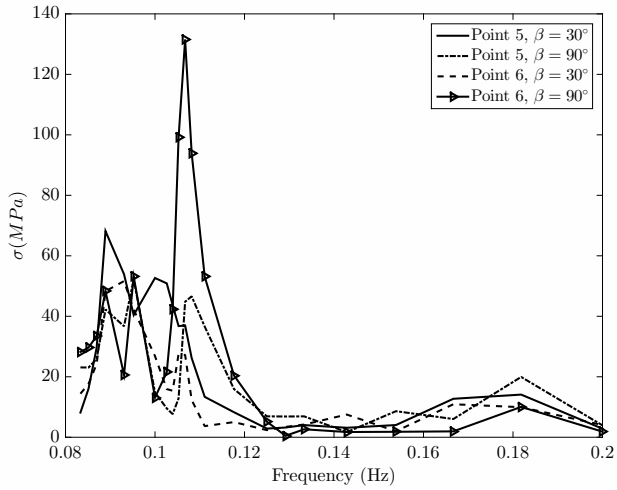


**FIGURE 13**. Structural stress computed at point 5 & 6 (Shown in Fig.7) for two incoming wave angles, illustrated in Fig.7.

We expect smaller stresses if larger thickness is used. The obtained peaks in shear stress are of valuable information as it determines which parts of the structure will need extra reinforcement.

## Conclusions

In this study, a preliminary hydroelastic analysis of a novel multi-wind-turbine floating platform is performed by use of the combined linear diffraction theory and Finite Element Method. The structure is designed to accommodate multiple turbines, and it rotates in response to the environmental loads. Considering the characteristics of the structure, it is critical to determine the response of the body to coupled loads. In this work, we have focused on the hydrodynamic loads. The structural responses of the platform and the vertical displacement for both rigid and flexible bodies are determined and discussed. Different responses are obtained for rigid and flexible cases, which shows the effect of considering the elasticity of the platform. However, the results need to be validated by experiments as well. Further investigation is required to ex-

amine the effect of various parameters on the structural response. Once an acceptable structural configuration is determined, the loads of the wind turbines will be added on the body and the coupled aero-, hydroelastic problem will be studied.


### Acknowledgements

This work is partially based on funding from the CBJ-Kaluosi-Qianghai Group of Hong Kong. This funding is gratefully acknowledged. Any findings and opinions contained in this present paper are those of the author and do not necessarily reflect the opinions of the funding company. The assistance of Professor H. Ronald Riggs of the University of Hawaii's Civil and Environmental Engineering Department, received during the course of HYDRAN computations, is greatly appreciated.


### REFERENCES


[1] World Energy Council, 2016. *World Energy Resources 2016*. World Energy Council, London,United Kingdom.

[2] Joao, C., and Atcheson, M., 2016. *Floating Offshore Wind Energy*. Green Energy and Technology. Springer International Publishing, Lisbon, Portugal.

[3] Castro-santos, L., 2016. *Floating Offshore Wind Farms*. Green Energy and Technology. Springer International Publishing, Ferrol, Spain.

[4] Henderson, A., Collu, M., and Masciola, M., 2016. "Overview of floating offshore wind technology". In *Floating Offshore Wind Energy, The Next Generation of Wind Energy, Edts. Cruz, j. and Atcheston, M.*, Vol. 1. Springer, pp. 87–123.

[5] Musial, W., Butterfield, S., and Boone, A., 2004. "Feasibility of Floating Platform Systems for Wind Turbines". In 23rd ASME Wind Energy Symposium, Reno, Nevada, USA, pp. 476–486.

[6] Ishihara, T., Phuc, P. V., Sukegawa, H., Shimada, K., and Ohyama, T., 2007. "A study on the dynamic response of a semi-submersible floating offshore wind turbine system Part 1: A water tank test". In Proceedings of the 12th International Conference on Wind Engineering, Cairns, Australia, pp. 2511–2518.

[7] Wong, C., 2015. "Wind tracing rotational semi-submerged raft for multi-turbine wind power generation". In EWEA Offshore 2015 Conference, Copenhagen, Denmark, pp. 1–10.

[8] Newman, J.N, 1994. *Marine Hydrodynamics*. MIT Press, Cambridge.

[9] Faltinsen, O, 1994. *Sea Loads on Ships and Offshore Structures*. Cambridge University Press, Cambridge ; New York.

[10] Faltinsen, O. M., 1990. "Wave Loads on Offshore Structures". *Annual Review of Fluid Mechanics,* ***22***, pp. 35–56.

[11] Huang, L. L., and Riggs, H. R., 2000. "The hydrostatic stiffness of fexible foating structures for linear hydroelasticity". *Marine Structures,* ***13***, pp. 91–106.

[12] Newman, J., 1994. "Wave effects on deformable bodies". *Applied Ocean Research,* ***16***(1), pp. 47–59.

[13] Riggs, R., 2005. HYDRAN:A Computer Program for the Hydroelastic response Analysis of Ocean Structures. Tech. rep., OffCoast.

[14] Riggs, H. R., Niimi, K. M., and Huang, L. L., 2007. "Two Benchmark Problems for Three-Dimensional, Linear Hydroelasticity". *Journal of Offshore Mechanics and Arctic Engineering,* ***129***(3), pp. 149–157.

[15] Riggs, H. R., Suzuki, H., Ertekin, R. C., Kim, J. W., and Iijima, K., 2008. "Comparison of hydroelastic computer codes based on the ISSC VLFS benchmark". *Ocean Engineering,* ***35***(7), pp. 589–597.

[16] Fugro GEOS Ltd, 2001. Wind and Wave Frequency Distribution for sites around the British Isles. Tech. rep., Southampton Oceanography Center, Southampton, United Kingdom.

[17] Mosley, B., Bungey, J., and Hulse, R., 2012. *Reinforced Concrete Design to Eurocode 2*, seventh ed. Mcmillan Publishers Ltd, Earthscan, International Institute for Environment and Development, London, United Kingdom.